

# Spin and Conductance-Peak-Spacing Distributions in Large Quantum Dots: A Density Functional Theory Study

Hong Jiang,<sup>1,2,3</sup> Harold U. Baranger,<sup>2,\*</sup> and Weitao Yang<sup>1,†</sup>

<sup>1</sup>*Department of Chemistry, Duke University, Durham, North Carolina 27708-0354*

<sup>2</sup>*Department of Physics, Duke University, Durham, North Carolina 27708-0305*

<sup>3</sup>*College of Chemistry and Molecular Engineering, Peking University, Beijing, China 100871*

(Dated: February 1, 2008)

We use spin-density-functional theory to study the spacing between conductance peaks and the ground-state spin of 2D model quantum dots with up to 200 electrons. Distributions for different ranges of electron number are obtained in both symmetric and asymmetric potentials. The even/odd effect is pronounced for small symmetric dots but vanishes for large asymmetric ones, suggesting substantially stronger interaction effects than expected. The fraction of high-spin ground states is remarkably large.

PACS numbers: 73.23.Hk, 73.40.Gk, 73.63.Kv

The interplay of quantum mechanical interference and electron-electron interactions is a current theme in many areas of solid-state physics: the 2D metal-insulator transition, interaction corrections in mesoscopic systems, and efforts toward solid-state quantum computing, for instance. A semiconductor quantum dot (QD) [1, 2] – a nano-device in which electron motion is quantized in all three dimensions – is a particularly simple system in which to study this interplay. In Coulomb blockade experiments in the electron tunneling regime, the conductance through the dot varies strongly as a function of gate voltage, forming a series of sharp peaks. For closed dots at low temperature, both the positions and heights of the peaks encode information about the dot's ground state. In particular, the spacing between adjacent conductance peaks is proportional to the second difference of the ground state energy with respect to electron number  $N$ ,  $\Delta_2 E(N) \equiv E_{gs}(N+1) + E_{gs}(N-1) - 2E_{gs}(N)$ , which is often called the addition energy. Furthermore, the ground state spin of the QD can be inferred from the shift in position of the conductance peaks upon applying a magnetic field.

The addition energy varies because of changing interference conditions either as  $N$  changes or from dot to dot, leading to a conductance-peak-spacing distribution. Previous theoretical work addressing this distribution can be divided into roughly two types: First, computational approaches addressed small dots with randomly disordered potentials – both exact diagonalization [3, 4, 5] and self-consistent field methods (Hartree-Fock [6, 7, 8, 9, 10] or density functional theory [11, 12]). Second, a semi-analytic treatment of large dots was developed based on general statistical assumptions [2, 13, 14, 15, 16, 17]: An important contribution to the variation comes from the single-particle energy; to treat this for irregular quantum dots, one assumes that the single-particle dynamics is classically chaotic, and so the single-particle quantum properties can be described by random matrix theory (RMT) [2, 18]. A random-phase approximation (RPA) treatment of the screened electron-electron interaction was then combined with such an RMT description of single-particle states to describe dots with large  $N$ .

The results of these two approaches are quite different.

First, for the zero temperature peak-spacing, the small dot calculations yield Gaussian-like distributions while the large  $N$  results are non-Gaussian. Second, spin degeneracy causes a significant “even/odd effect” in the large dot approach: the distribution for  $N$  even is very different from that for  $N$  odd. Third, with regard to the ground state spin [12, 19, 20, 21, 22], the small  $N$  calculations find an enhancement of the low spin states compared to the large QD approach.

Experimental work to date [3, 23, 24, 25, 26] has unfortunately failed to probe the ground state addition energy distribution or ground state spin of generic systems. In the more recent experiments, either temperature obscured the ground state properties [15, 16, 24, 26] or the dot was regular in shape [25].

Our aim here is to bridge the gap between the two theoretical approaches and in so doing highlight the need for more experiments. We have used the Kohn-Sham (KS) spin density-functional theory (SDFT) [27] to study both the peak-spacing and the spin distribution for 2D model QDs. Using an efficient algorithm [35], we obtain statistics with  $N$  up to 200. This is the first calculation, as far as we know, for large realistic QDs.

Our primary result is that the effective electron-electron interaction that emerges is substantially stronger than that predicted from the RPA-RMT treatment. The evidence is two-fold: (1) the addition energy distribution is Gaussian-like with no discernible even/odd effect, and (2) the probability of having a high spin state ( $S \geq 1$ ) is larger than the maximum possible from RPA-RMT.

In SDFT, the energy of the interacting system is expressed as a functional of the spin up ( $\alpha$ ) and down ( $\beta$ ) electron densities,  $\rho_\alpha(\mathbf{r})$  and  $\rho_\beta(\mathbf{r})$ . (Effective atomic units are used: for GaAs-AlGaAs QDs, the values are 10.08 meV for energy and 10.95 nm for length.) The functional is built out of four parts. Two are trivial – the response to the external potential  $V_{ext}$  and the Coulomb energy. The kinetic energy of a non-interacting reference system is included explicitly:  $T_s[\rho_\alpha, \rho_\beta] = \sum_{i,\sigma} \langle \psi_{i\sigma} | -\frac{1}{2} \nabla^2 | \psi_{i\sigma} \rangle$  with  $\rho_\sigma = \sum_i |\psi_{i\sigma}|^2$  and  $\sigma = \alpha, \beta$ . The final term is, of course, the exchange-correlation energy  $E_{xc}[\rho_\alpha, \rho_\beta]$ . Thus the KS-SDFT func-

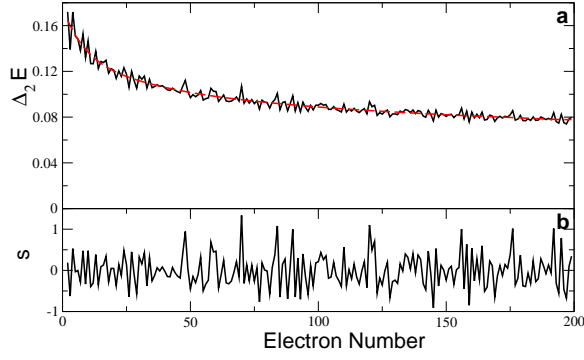


FIG. 1: Addition energy as a function of electron number. (a) Raw addition energy data (solid) and its polynomial fit (dashed) to remove the change in classical charging energy. (b) Addition energies scaled by the mean level-spacing after removing smooth part. ( $\lambda = 0.6$  and  $\gamma = 0$ .)

tional is

$$E[\rho_\alpha, \rho_\beta] = T_s[\rho_\alpha, \rho_\beta] + \int V_{ext}(\mathbf{r})\rho(\mathbf{r})d\mathbf{r} + \int \frac{\rho(\mathbf{r})\rho(\mathbf{r}')}{|\mathbf{r} - \mathbf{r}'|}d\mathbf{r}d\mathbf{r}' + E_{xc}[\rho_\alpha, \rho_\beta]. \quad (1)$$

The ground state energy is obtained by minimizing the functional with respect to the spin densities under the constraints  $\int \rho_\sigma(\mathbf{r})d\mathbf{r} = N_\sigma$ . We use the standard local spin density approximation (LSDA) for  $E_{xc}$  which works well in various semiconductors; in particular, we use Tanatar and Ceperley's 2D parametrization [28]. For 2D clean QDs, comparisons with quantum Monte-Carlo calculations for  $N \leq 8$  and interaction strength parameter  $r_s \leq 8.0$  have shown that LSDA works well for both the ground state spin and energy [29, 30].

We use a quartic potential to model 2D QD systems,

$$V_{ext}(\mathbf{r}) = a\left[\frac{x^4}{b} + by^4 - 2\lambda x^2 y^2 + \gamma(x^2 y - xy^2)r\right]. \quad (2)$$

Both the classical dynamics and the single-particle quantum mechanics at  $\gamma = 0$  have been studied in detail [31]: the system evolves continuously from integrable to fully chaotic as  $\lambda$  changes from 0 to 1. The parameter  $\gamma$  breaks the four-fold symmetry. The prefactor is  $a = 1.0 \times 10^{-4}$ ; this allows the electrons to spread so that the interaction strength parameter,  $r_s$ , is about 1.5, close to experimental conditions.

For a given  $V_{ext}$ , we calculate the total energy at several values of electron number  $N$  and total spin  $S$ . Selecting the minimum energy determines the ground state energy  $E_{gs}$  and spin  $S_{gs}$  as a function of  $N$ . The addition energy is then calculated as the second difference of  $E_{gs}(N)$ ; an example is shown in Fig. 1(a). To obtain good statistics, in both the symmetric and asymmetric cases we calculate five sets of data with different parameters [36]. A correlation analysis shows that both the single-particle level spacing (SPLS) and addition energy from the different sets are statistically independent.

Since the slow decrease in  $\Delta_2 E(N)$  is a classical effect – the increasing capacitance as the dot becomes bigger – we

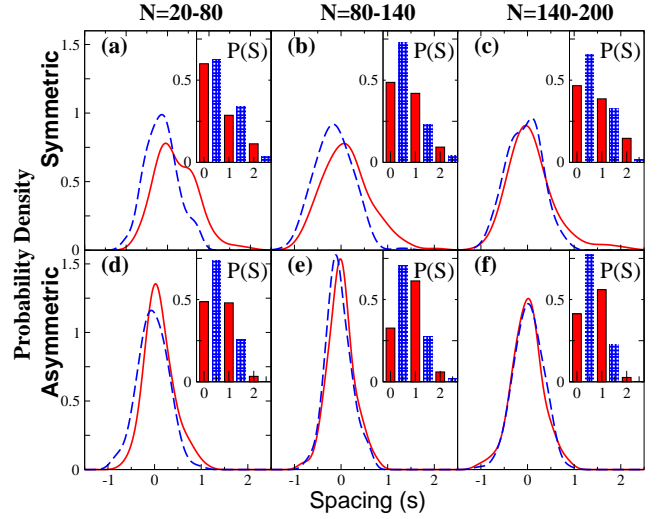


FIG. 2: Distributions of peak-spacing,  $s$ , for even (solid) and odd (dashed)  $N$ . The columns correspond to the different ranges of electron number indicated, while the first row [(a)-(c)] is for a symmetric external potential and the second for asymmetric [(d)-(f)]. The inset of each figure shows the corresponding spin distribution for  $N$  even (solid) and odd (skeleton). Both the lack of even/odd effect and the large spin in panel (f) is striking and indicates an unexpectedly large effective electron-electron interaction. (A sliding window is used in estimating the probability density, yielding a smooth curve rather than a histogram; each curve is made from 150 data points using a Gaussian window of width 0.3.)

remove it by fitting a polynomial to find the smooth part  $\langle \Delta_2 E(N) \rangle$ . To compare with experiments, the addition energy is scaled by the mean-level spacing found from the average electron density  $n$  through  $\Delta = 2\pi\hbar^2\langle n \rangle/m^*N$ . The resulting dimensionless spacing is denoted  $s \equiv [\Delta_2 E(N) - \langle \Delta_2 E(N) \rangle]/\Delta$ ; see Fig. 1(b). Note that the typical scale of  $s$  is 1; that is, fluctuations of the addition energy are on the scale of the single-particle mean-level spacing.

We find the distribution of  $s$  for even and odd  $N$  in three ranges of electron number,  $N = 20-80$ ,  $80-140$ , and  $140-200$ , in both symmetric and asymmetric external potentials. (For the smallest, mean, and largest values of  $N$ ,  $r_s$  is 2.5, 1.6, and 1.4, respectively.) The main features of the results, shown in Fig. 2, are as follows. (1) *Even/odd*: There is a difference in the distribution for  $N$  even or odd in the small  $N$  range, and the parity effect in the symmetric case is more pronounced than for asymmetric potentials. But there is a striking *absence* of even/odd effect in the asymmetric large  $N$  case [panel (f)]. (2) *Shape*: The distributions are Gaussian-like. This extends the previous small  $N$  results, disagrees with the RPA-RMT results for large  $N$ , and is consistent with experiments [24, 26] (where, however, the ground state properties are obscured by temperature effects [15, 16]). (3) *Small/large*: The spacing distributions for small  $N$  are different from those for large  $N$ . Since the experimental QDs generally involve tens to hundreds of electrons, one must be cautious in generalizing to large dots conclusions drawn from studying small dots.

(4) *Symmetric/Asymmetric*: Both the variance of the peak-spacing and the magnitude of the even/odd effect is larger in the symmetric case.

The insets in Fig. 2 show histograms of the spin distribution for the corresponding electron number ranges. A remarkable feature is the significantly *higher* fraction of high spin ground states that we find at large  $N$  than in either previous SDFT investigations of small disordered dots [12] (for small  $N$ , we agree, of course, with previous results) or other investigations. Especially in the asymmetric case,  $P(S=1)$  is even higher than  $P(S=0)$  for  $N=80$ -200! Again we see a clear dependence on the electron number range: while the spin distribution for odd  $N$  changes little as  $N$  increases, the spin distribution for even  $N$  is quite different for small and large  $N$ . Comparing spin distributions in the presence and absence of symmetry, we see a larger high-spin fraction in the asymmetric case for all three ranges of  $N$ .

This last result is at first surprising: generally one expects increased symmetry to increase the spin – as in Hund’s rule for the spin of atoms. We can use random matrix theory, however, to show that there are competing effects here – namely the statistics of the eigenenergies vs. the statistics of the eigenfunctions. For simplicity we consider the simplest RMT: a two-electron two-level model in which we neglect spatial correlations beyond a wavelength. In a Hartree-Fock framework and under the assumption that the orbitals remain the same for different spin configurations, the energy difference between the singlet ( $S=0$ ) and triplet ( $S=1$ ) states is

$$\delta E \equiv E_{S=1} - E_{S=0} = \delta\epsilon + (J_{12} - K_{12}) - J_{11}, \quad (3)$$

where  $\delta\epsilon$  is the single-particle level spacing,  $J_{ij} = \int d\mathbf{r} d\mathbf{r}' |\psi_i(\mathbf{r})|^2 v_{scr}(\mathbf{r}, \mathbf{r}') |\psi_j(\mathbf{r}')|^2$  are the Coulomb energies, and  $K_{12} = \int d\mathbf{r} d\mathbf{r}' \psi_1^*(\mathbf{r}) \psi_2^*(\mathbf{r}') v_{scr}(\mathbf{r}, \mathbf{r}') \psi_1(\mathbf{r}') \psi_2(\mathbf{r})$  is the exchange energy. Here instead of using the bare Coulomb interaction, we use the screened potential  $v_{scr}(\mathbf{r}, \mathbf{r}')$  in order to implicitly account for the other electrons. Qualitatively, the screened interaction is approximately zero-range,  $v_{scr}(\mathbf{r}, \mathbf{r}') \rightarrow (A\Delta/2)\delta(\mathbf{r} - \mathbf{r}')$  where  $\Delta$  is the mean single-particle level spacing and  $A$  is the area. In this limit, the second term in Eq. (3) vanishes, and the third term is proportional to the “inverse participation ratio” (IPR) defined by  $I \equiv A \int d\mathbf{r} |\psi(\mathbf{r})|^4$ . Therefore, in the zero-range limit and considering the time-reversibility of the system [37], we have

$$\delta E_{\text{zero-range}} = \delta\epsilon - I\Delta/3. \quad (4)$$

There is clearly a competition here between the level spacing – a large spacing tends to decrease the spin – and the statistics of the wave functions – increased localization increases  $I$  and leads to a large spin.

To see the competition explicitly, we calculate the distribution of the SPLS  $\delta\epsilon$  and that of the IPR from top-level KS orbital energies and wave functions in both the symmetric and asymmetric cases. Results are shown in Fig. 3. While the symmetric case has a higher probability of small level-spacing, the mean value of the IPR is also smaller in the symmetric case. Our overall result for the spin distribution – the

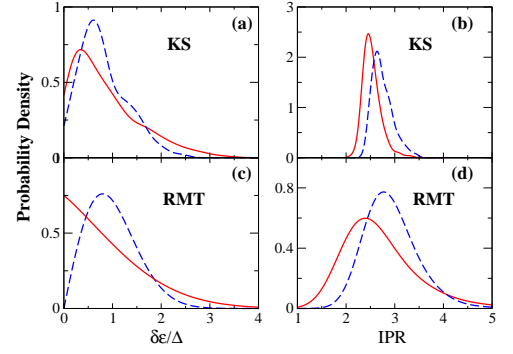


FIG. 3: Distributions of the single-particle level spacing (scaled by the mean) and the IPR from Kohn-Sham calculations and from random matrix theory. (a) The distribution of SPLS calculated from top KS orbital energies for symmetric (solid) and asymmetric (dashed) case respectively. (b) The distribution of IPR calculated from top-level KS orbital wave functions for symmetric (solid) and asymmetric (dashed) case respectively. (c) The distributions of SPLS for a single GOE (dashed) and the superposition of four GOE (solid) according to RMT. (d) The distributions of IPR calculated from the eigenvectors of real symmetric random matrix with dimension  $M=20$  (solid) and  $M=80$  (dashed).

decrease in probability of  $S=1$  upon introducing symmetry [Fig. 2(f)] – shows that the effect of wave function statistics is stronger in our system.

The trend here is captured by the random matrix theory. For an asymmetric chaotic external potential, the distribution of the SPLS is that of the Gaussian orthogonal ensemble (GOE). In the symmetric chaotic case, however, the SPLS statistics is the superposition of four GOE’s [18], one for each symmetry class. Fig. 3(c) shows these two distributions. Clearly, the superposition greatly reduces the nearest-neighbor level repulsion, which implies that spatial symmetry favors a high-spin ground state, in accordance with Hund’s rule.

For the wave function statistics, RMT suggests that the single-particle wave functions of classically chaotic systems are described by  $M$ -dimensional random unit vectors [2, 32]. The shape of the resulting distribution of IPR depends on  $M$ , as shown in Fig. 3(d) for  $M=20$  and 80. These values of  $M$  are chosen to correspond to the number of independent orbital levels: approximately  $N/2$  in the asymmetric case because of spin, and  $N/8$  for the four-fold symmetric external potential. Symmetry reduces the effective  $M$  and so reduces the IPR, acting against a high-spin ground state. Hence there is a competition between the SPLS and the IPR.

Note that the dependence of the IPR on  $M$  also explains the change in the spin distribution as electron number varies: The wave functions for small  $N$  have a smaller effective  $M$ , hence a smaller IPR. Thus a low-spin ground state is more favorable. Similarly, a three-level analysis provides a qualitative explanation of odd  $N$  results.

The results in Fig. 3 show, of course, that the calculated distributions of both the SPLS and the IPR agree with RMT only qualitatively. The fluctuation of the IPR is particularly

striking: it is much smaller for the KS wave functions than in RMT. We believe this is due to the neglect of spatial correlations in our very simple RMT.

In summary, by studying a model 2D quantum dot with up to  $N = 200$  electrons, we have found new phenomena. Both the statistics of ground state spin and the spacing between conductance peaks depend on the electron number, as well as on the spatial symmetry. The results for large electron number and asymmetric potential are surprising: the shape of the peak-spacing distribution is Gaussian-like, the even/odd effect vanishes, and there is a substantial fraction of large spin ground states ( $S \geq 1$ ). These effects imply a strong effective or residual electron-electron interaction.

This is remarkable considering that conditions in our dots are not extreme:  $r_s \sim 1.5$  corresponds to a moderate bare interaction strength, and the dimensionless conductance is large,  $g \sim 4$ . In fact, previous work using the RPA-RMT approach suggested that we should obtain a strong even/odd effect [14, 16]. Conversely, to obtain the spin and peak-spacing distributions that we find here from the RPA-RMT model requires an effective exchange constant of  $J_s \sim 0.6\Delta$ , larger than the maximum value possible in RPA. The origin of this unexpectedly large residual interaction is not presently known, and we leave it for future investigation.

We close with a caveat and a comment: First, this work is based on the 2D local spin density approximation whose validity, though already verified for *small* parabolic QD's [29, 30], is not well tested for *large* non-parabolic quantum dots as studied here. Our result highlights the need to go beyond RPA-RMT and perform a real Fermi liquid theory study. On the other hand, note the recent experimental work in Ref. 33 which, though still preliminary because of insufficient data, indicates a high probability of large-spin ground states. The surprisingly large effective interactions found here suggest that more experiments should be a high priority.

We appreciate discussions with D. Ullmo and G. Usaj. This work was supported in part by NSF Grant No. DMR-0103003 and the North Carolina Supercomputing Center.

---

\* baranger@phy.duke.edu

† weitaoyang@duke.edu

- [1] L. P. Kouwenhoven, C. M. Marcus, P. L. McEuen, S. Tarucha, R. M. Wetervelt, and N. S. Wingreen, in *Mesoscopic electron transport*, edited by L. L. Sohn, G. Schön, and L. P. Kouwenhoven (Kluwer, Dordrecht, 1997), pp. 105–214.
- [2] Y. Alhassid, *Rev. Mod. Phys.* **72**, 895 (2000).
- [3] U. Sivan, R. Berkovits, Y. Aloni, O. Prus, A. Auerbach, and G. Ben-Yoseph, *Phys. Rev. Lett.* **77**, 1123 (1996).
- [4] O. Prus, A. Auerbach, Y. Aloni, U. Sivan, and R. Berkovits, *Phys. Rev. B* **54**, 14289 (1996).
- [5] R. Berkovits, *Phys. Rev. Lett.* **81**, 2128 (1998).
- [6] A. Cohen, K. Richter, and R. Berkovits, *Phys. Rev. B* **60**, 2536 (1999).
- [7] P. N. Walker, G. Montambaux, and Y. Gefen, *Phys. Rev. B* **60**, 2541 (1999).
- [8] S. Levit and D. Orgad, *Phys. Rev. B* **60**, 5549 (1999).
- [9] K. Ahn, K. Richter, and I. Lee, *Phys. Rev. Lett.* **83**, 4144 (1999).
- [10] L. Bonci and R. Berkovits, *Europhys. Lett.* **47**, 708 (1999).
- [11] M. Stopa, *Phys. Rev. B* **54**, 13767 (1996).
- [12] K. Hirose and N. S. Wingreen, *Phys. Rev. B* **65**, 193305 (2002).
- [13] Y. M. Blanter, A. D. Mirlin, and B. A. Muzykantskii, *Phys. Rev. Lett.* **78**, 2449 (1997).
- [14] D. Ullmo and H. U. Baranger, *Phys. Rev. B* **64**, 245324 (2001).
- [15] G. Usaj and H. U. Baranger, *Phys. Rev. B* **64**, 201319 (2001).
- [16] G. Usaj and H. U. Baranger (2002), arXiv:cond-mat/0203074.
- [17] I. L. Aleiner, P. W. Brouwer, and L. I. Glazman, *Phys. Rep.* **358**, 309 (2002).
- [18] O. Bohigas, in *Chaos and Quantum Physics*, edited by M. J. Giannoni, A. Voros, and J. Jinn-Justin (North-Holland, Amsterdam, 1990), pp. 87–199.
- [19] P. W. Brouwer, Y. Oreg, and B. I. Halperin, *Phys. Rev. B* **60**, R13 977 (1999).
- [20] I. L. Kurland, I. L. Aleiner, and B. L. Altshuler, *Phys. Rev. B* **62**, 14886 (2000).
- [21] P. Jacquod and A. D. Stone, *Phys. Rev. B* **64**, 214416 (2001).
- [22] Y. Oreg, P. W. Brouwer, X. Waintal, and B. I. Halperin (2001), arXiv:cond-mat/0109541.
- [23] F. Simmel, T. Heinzl, and D. A. Wharam, *Europhys. Lett.* **38**, 123 (1997).
- [24] S. R. Patel, S. M. Cronenwett, D. R. Stewart, A. G. Huibers, C. M. Marcus, C. I. Duruöz, J. S. Harris, J. K. Campman, and A. C. Gossard, *Phys. Rev. Lett.* **80**, 4522 (1998).
- [25] S. Lüscher, T. Heinzl, K. Ensslin, W. Wegscheider, and M. Bichler, *Phys. Rev. Lett.* **86**, 2118 (2001).
- [26] T. T. Ong, H. U. Baranger, D. M. Higdon, S. R. Patel, and C. M. Marcus (2001), unpublished.
- [27] R. G. Parr and W. Yang, *Density-Functional Theory of Atoms and Molecules* (Oxford University Press, New York, 1989).
- [28] B. Tanatar and D. M. Ceperley, *Phys. Rev. B* **39**, 5005 (1989).
- [29] R. Egger, W. Häusler, C. H. Mak, and H. Grabert, *Phys. Rev. Lett.* **82**, 3320 (1999).
- [30] F. Pederiva, C. J. Umrigar, and E. Lipparini, *Phys. Rev. B* **62**, 8120 (2000).
- [31] O. Bohigas, S. Tomsovic, and D. Ullmo, *Phys. Rep.* **223**, 43 (1993).
- [32] N. Ullah, *Nucl. Phys.* **58**, 65 (1964).
- [33] J. A. Folk, C. M. Marcus, R. Berkovits, I. L. Kurland, I. L. Aleiner, and B. L. Altshuler, *Phys. Scripta* **T90**, 26 (2001).
- [34] M. C. Payne, M. P. Teter, D. C. Allan, T. A. Arias, and J. D. Joannopoulos, *Rev. Mod. Phys.* **64**, 1045 (1992).
- [35] In our program, the wave functions are represented in real space, and the kinetic energy operator is applied using a fast-sine transform. The Hartree potential is calculated using Fourier convolution. The KS equations are solved by a direct minimization preconditioned conjugate-gradient method [34].
- [36] The parameter values used in our calculations are as follows: In all cases,  $a = 1.0 \times 10^{-4}$  and  $b = \pi/4$ . For the symmetric case  $\gamma = 0$ , we take  $\lambda$  to be 0.53, 0.6, 0.67, 0.74, and 0.81. For the asymmetric case we choose five sets of  $(\lambda, \gamma)$ : (0.53, 0.1), (0.565, 0.2), (0.6, 0.1), (0.635, 0.15), and (0.67, 0.1).
- [37] In the time-reversal symmetric case, there are three contributions to the average IPR, the direct, exchange, and Cooper pairings. However, when using the IPR to estimate the magnitude of interaction effects, one must keep in mind that higher-order processes in the screened interaction may renormalize the magnitude. This is well-known for the Cooper channel; since its final magnitude is small, it should be neglected. We take this into account by using  $2I/3$  in the estimate of the interaction effect rather than the full  $I$ .